

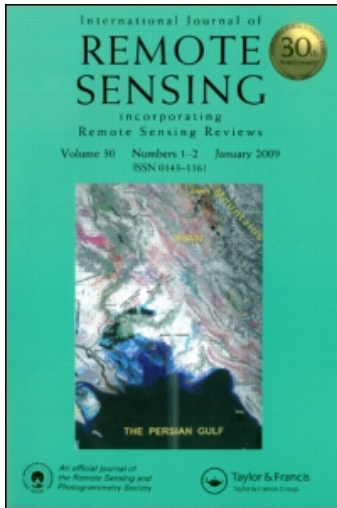
This article was downloaded by: [IFREMER Bibliothèque La Pérouse - Centre de Documentation de la mer]

On: 6 November 2010

Access details: Access Details: [subscription number 919230466]

Publisher Taylor & Francis

Informa Ltd Registered in England and Wales Registered Number: 1072954 Registered office: Mortimer House, 37-41 Mortimer Street, London W1T 3JH, UK



International Journal of Remote Sensing

Publication details, including instructions for authors and subscription information:

<http://www.informaworld.com/smpp/title~content=t713722504>

Validation and intercomparison of ocean wave spectra inversion schemes using ASAR wave mode data

Xiaoming Li^a; Thomas Koenig^a; Johannes Schulz-Stellenfleth^b; Susanne Lehner^a

^a German Aerospace Center (DLR), Oberpfaffenhofen, Wessling, Germany ^b GKSS Research Center Geesthacht, Max-Planck-Straße 1, Geesthacht, Germany

Online publication date: 28 September 2010

To cite this Article Li, Xiaoming , Koenig, Thomas , Schulz-Stellenfleth, Johannes and Lehner, Susanne(2010) 'Validation and intercomparison of ocean wave spectra inversion schemes using ASAR wave mode data', International Journal of Remote Sensing, 31: 17, 4969 – 4993

To link to this Article: DOI: 10.1080/01431161.2010.485222

URL: <http://dx.doi.org/10.1080/01431161.2010.485222>

PLEASE SCROLL DOWN FOR ARTICLE

Full terms and conditions of use: <http://www.informaworld.com/terms-and-conditions-of-access.pdf>

This article may be used for research, teaching and private study purposes. Any substantial or systematic reproduction, re-distribution, re-selling, loan or sub-licensing, systematic supply or distribution in any form to anyone is expressly forbidden.

The publisher does not give any warranty express or implied or make any representation that the contents will be complete or accurate or up to date. The accuracy of any instructions, formulae and drug doses should be independently verified with primary sources. The publisher shall not be liable for any loss, actions, claims, proceedings, demand or costs or damages whatsoever or howsoever caused arising directly or indirectly in connection with or arising out of the use of this material.

Validation and intercomparison of ocean wave spectra inversion schemes using ASAR wave mode data

XIAOMING LI†*, THOMAS KOENIG‡,

JOHANNES SCHULZ-STELLENFLETH‡ and SUSANNE LEHNER†

†German Aerospace Center (DLR), Oberpfaffenhofen, 82234 Wessling, Germany

‡GKSS Research Center Geesthacht, Max-Planck-Straße 1, 21502 Geesthacht, Germany

This paper presents a validation and intercomparison of the non-linear Partition Rescaling and Shift Algorithm (PARSA) for deriving full two-dimensional ocean wave spectra from ENIVSAT Advanced Synthetic Aperture Radar (ASAR) Wave Mode (WM) data.

ASAR WM data acquired globally are used for the validation exercise by comparing the retrieved significant wave height (SWH), zero up-crossing wave period (T_{m02}), swell SWH (H_{12} , for waves with a period longer than 12 s), mean wave frequency and mean wave direction to *in situ* buoy measurements and results from the European Centre for Medium-Range Weather Forecast (ECMWF) reanalysis wave model and the Deutscher Wetterdienst (DWD) forecast wave model.

An intercomparison of results from the PARSA algorithm with those from the quasi-linear retrieval algorithm adopted by the European Space Agency (ESA) to generate the ASAR WM level-2 product (ASA_WVW_2P, termed WVW hereafter) is also presented in this paper. In addition to the intercomparison with the existing ASAR WM WVW product, sea state parameters (SWH and T_{m02}), integrated from the PARSA spectra are also compared to the results derived using the empirical algorithm CWAVE_ENV.

Validation results indicate that the PARSA inversion can yield full two-dimensional ocean wave spectra. The retrieved SWH corresponds well to buoy measurements with a scatter index of 21%, as demonstrated by 1247 collocated data pairs. By comparing SWH to the ECMWF reanalysis wave model and the DWD forecast wave model, better agreement is achieved, with scatter indices of 9% and 16%, respectively.

In addition to comparing conventional integral wave parameters normally used to assess the quality of inverted spectra, a comparison of individual PARSA spectra chosen in different sea state with the nearest numerical wave model spectra and the WVW spectra is performed to illustrate two-dimensional spectral differences.

1. Introduction

Because SAR can operate independent of weather conditions and sunlight to provide two-dimensional backscatter information over the sea surface, it is particularly useful to derive two-dimensional surface wave information. This information is generally not easily acquired by *in situ* buoy measurements. There are few data available from directional wave buoys in the open sea. Most measurements are from locations near the coast and are often just frequency spectra that lack directional information.

*Corresponding author. Email: Xiao.Li@dlr.de

Although numerical wave models may produce directional wave information, wave models are not perfect as their quality is limited by the model configuration and the input wind forcing.

The European Remote Sensing Satellite (ERS-1/2) and the Environmental Satellite (ENVISAT), launched in 1991, 1995 and 2002, respectively, have provided SAR Wave Mode (WM) data on a global and continuous basis. These data are particularly valuable in validating global wave models and in improving wave forecast through assimilation approaches.

The basic principles of SAR imaging of the ocean surface were discussed in Alpers *et al.* (1981) and Hasselmann *et al.* (1985). According to the latter article, three processes contribute to ocean wave imaging by SAR systems: (i) hydrodynamic modulation, whereby the amplitude of the capillary waves is modulated by long waves; (ii) tilt modulation, whereby the sea surface slope is changed by long waves. Both modulations are recognized as linear modulations for Real Aperture Radar (RAR); and (iii) the Doppler shift in the return signal produced by the long wave orbital velocity, which leads to the azimuth displacement of scatter elements in the image plane. The density of the scatter elements varies in the azimuth direction and thus produces a wave-like pattern in SAR images. This effect (known as velocity bunching) plays an important role in wave components travelling in azimuth directions, see as well Lyzenga *et al.* (1985).

In addition to the modulations mentioned above, the effect of foreshortening can also contribute to the wave-like pattern visible in SAR images, as first pointed out in Gower (1983). This effect, also referred to as 'range bunching', was the subject of theoretical investigations in which it was found that the range bunching depends on the local wave height and that it can enhance the tilt modulation up to 50% in high sea state (Ouchi 1988).

An initial derivation of the full two-dimensional ocean wave spectra from SAR imagery is published in Hasselmann and Hasselmann (1991) at the Max-Planck Institute (MPI) for Meteorology; they were then refined by Krogstad (1992) and further upgraded by Hasselmann *et al.* (1996). The scheme involves taking prior information from a numerical wave model as an additional input to overcome the 180° directional ambiguity of wave travel and supplement the missing SAR information beyond the azimuthal cut-off. An assessment of the quality of the retrieval wave spectra and the operational feasibility of this scheme was presented in Heimbach *et al.* (1998); these authors used 3 years' worth (1993–1995) of ERS-1 SAR WM User Wave (UWA) spectral data (i.e. SAR image spectrum; see Brooker 1995). Validation results indicate that approximately 75% of the SAR WM spectral data were converted to successful retrievals. A small overestimation of less than 0.5 m for significant wave height (SWH) by the MPI was observed when compared to the Wave Model.

Using the additional phase information in the SAR single look complex data, the SAR look cross spectra (SLCS) are used to eliminate directional ambiguity. Applications of the SLCS approach for wind and wave measurements have been investigated using the reprocessed ERS-2 SAR WM data (Lehner *et al.* 2000, Li *et al.* 2008). From the ENVISAT mission, the SLCS data are provided operationally as the ASAR WM level-1b product, termed WVS.

A scheme for retrieving ocean wave spectra without directional ambiguity based on airborne SAR cross-spectral data has been suggested by Engen and Johnsen (1995). This scheme is as used to extract two-dimensional wave measurements operationally

from the ENVISAT ASAR WM data (Chapron *et al.* 2001) and deliver it to users as the standard level-2 product, WWV.

Over the open water, the SAR/ASAR instruments are operated in WM whenever no other operation is requested. In WM, the SAR sensor collects data to form small images of $10 \text{ km} \times 5 \text{ km}$ every 200 or 100 km along the satellite's orbit. These WM data offer global coverage and have received considerable attention in the development of SAR inversion algorithms and data assimilation, particularly when the data and high-level product (WWV) are provided operationally in the ENVISAT mission.

Global validation of WWV product wave measurements have been carried out at various weather centres such as the European Centre for Medium-Range Weather Forecast (ECMWF) (Janssen *et al.* 2007, Abdalla *et al.* 2008) and the UK Met Office (Li and Holt 2009). As previously pointed out the WWV inverted wave spectra are not full two-dimensional ocean wave spectra, but they are limited by the so-called azimuth cut-off wavelength (typically longer than 200 m). Therefore, one has to restrict the comparisons to the inner part of the spectrum only, e.g. by comparing the swell wave height (H_{12}) to other observations or numerical wave models.

Comparisons indicate that the inverted WWV wave height is variable, with higher scatter indices of 44.8% (Janssen *et al.* 2007) and 46.9% (Abdalla *et al.* 2008) when compared to the ECMWF wave model during the periods of November 2005 to October 2006 and November 2006 to October 2007, respectively.

Using the numerical wave model run by the UK Met Office as a 'bridge' measurement, the sub-range wave height (SRWH) extracted from ASAR WM WWV products has been compared with data from three buoys (in Christmas Island, where long swell is expected, in the Gulf of Mexico, where only wind sea is expected, and near Cape San Martin, under mixed-wave conditions) (Li and Holt 2009). Validation exercises show that the quality of WWV product is worst for the range of wave period of 8–5 s, which is reasonable considering short waves are not resolved by the sensor. The 16–11 s bin shows relatively good agreement with the model results of UK Met Office. However, spurious wave energy is observed for waves with a longer period of 23–16 s.

To remove the strong variance of inverted wave height, the ASAR WM inversion algorithm was upgraded (Johnsen and Collard 2006); the upgraded algorithm has been in use since late October 2007. In a recent annual report of long-term quality assessment of WWV products (Johnsen and Collard 2009), H_{12} derived from the WWV products acquired during November 2007 to December 2008 was compared to buoy measurements. The RMSE and bias are 0.88 m and 0.16 m, respectively. The results changed to 0.66 and 0.32 m when taking into account only data acquired in weather conditions with wind speed below 10 m s^{-1} . When using a bias-extracting model given in Collard *et al.* (2009), the RMSE decreased to 0.35 m compared with buoy observations, due to the use of an even stronger restriction on wind speed (U_{10} has to be below 8 m s^{-1}).

Thus, assessment and validation of the quality of WWV products has shown that the inverted spectra are not available as full two-dimensional ocean wave spectra but are limited to the cut-off. The integrated wave parameters present the sea state resolved within the cut-off of the ASAR sensor and for cases of low wind speed.

As a potential higher-level product of ASAR WM, it was suggested that the PARSA scheme (Schulz-Stellenfleth *et al.* 2005) is to be used to retrieve full two-dimensional ocean wave spectra using the SLCS as an input in addition to first guess information. This method is particularly valuable for the validation and assimilation of numerical wave models. For validation of PARSA spectra with large entries, we do

not compare the spectra directly to other observations; instead we use the integrated wave parameters, including SWH, mean wave period and mean wave direction, to quantify the quality of inverted wave spectra.

The paper is structured as follows. In the second section, relevant datasets used for the validation study are introduced. In the third section of the paper, we present brief information on the non-linear mapping function of ocean wave spectra into SAR image spectra. This mapping function is also a basis used for generating the WWV products from the ASAR WM data. In the fourth section, we conduct the validation and intercomparison of the PARSA scheme and WWV products, by comparing integral wave parameters and individual inverted spectra to other observations, and present the results of these exercises. The conclusions and outlook are summarized in §5.

2. Description of relevant data

ASAR WM cross-spectral data, i.e. Level-1b WVS, are used as the input for the PARSA inversion scheme.

Some oceanic or atmospheric features such as oil slicks, sea ice, and atmospheric boundary roll are visible on ASAR WM data but are not relevant to measurement of ocean surface waves and may influence the SAR inversion results. Therefore, pre-processing using a homogeneity test (Schulz-Stellenfleth and Lehner 2004) is applied to exclude the inhomogeneous WM data and the corresponding inverted PARSA spectra.

Figure 1(a) shows an ASAR imagette with a homogeneous sea surface acquired over the South Atlantic on 22 February 2007. The global ASAR orbit on 22 February 2007 is also given for reference in Figure 1(b).

The ESA ASAR WWV products provide inverted two-dimensional ocean wave spectra on a log-polar grid with 24 wavelengths and 36 directions. The integrated SWH is also provided in the measurement dataset (MDS) of the WWV product.

The match-up dataset used to assess the quality of PARSA inversion spectra and the ESA WWV products, are collected from the ECMWF reanalysis wave model, the independent Deutscher Wetterdienst (DWD) forecast wave model, *in situ* buoy measurements and cross-over measurements from the radar altimeter (RA).

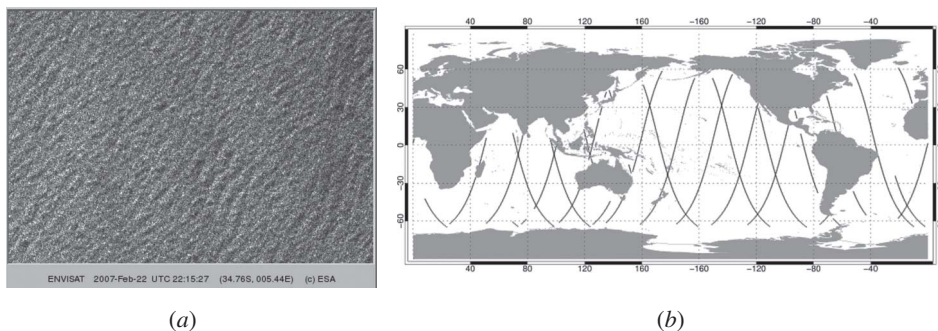


Figure 1. (a) The quicklook (8 bit grey scale) of an ASAR wave mode imagette with homogeneous wave patterns acquired on 22 February 2007 over the South Atlantic (© ESA); (b) the global ASAR track on 22 February 2007 is provided for reference.

2.1 Match-up dataset for validation

In addition to the input of SAR cross-spectral data, the PARSA inversion scheme also requires prior information, e.g. from numerical wave models. In this exercise, we choose the ECMWF reanalysis wave model results as the first guess information. The matched up ECMWF reanalysis wave model was acquired through the CERSAT collocation system with spatial and temporal resolution of 1.5° and 6 h, respectively.

We also collected the match-up dataset from the DWD forecast wave model, which is provided with 0.75° grid resolution and 3-h intervals.

Although they differ in their model configurations and forcing wind fields, the ECMWF and DWD wave models both use the third generation WAVE Model (WAM; WAMDI Group 1988) of version cycle 4 (Günther *et al.* 1992). It is worth noting that the ECMWF reanalysis wave model used for validation has already been assimilated with RA and ASAR WM cross-spectral data. The DWD wave model gives the forecast results. Only scatterometer data have been routinely assimilated into the atmospheric model used to force the WAM model. Due to the contribution of increased observations for sea state and surface wind field provided by satellites (e.g. RA, SAR and Scatterometer observations), the accuracy of the forecast numerical wave model has improved considerably (Janssen 2008).

Figure A1 in Appendix 1 shows a map of 77 buoys used for validation. Most of the buoys are deployed by the NOAA National Data Buoy Center (NDBC) and the Environment Canada Marine Environmental Data Service (MEDS). The names, longitudes and latitudes of these buoys are given in table A1.

RA measurements of SWH derived from Geosat Follow-On (GFO) and JASON are used as independent validation sources.

3. PARSA retrieval approach

The PARSA scheme is described to derive the complete two-dimensional ocean wave spectrum from SAR WM data with prior information obtained from a numerical wave model, e.g. the WAM model. Thus, the retrieved results present the best available estimation by making use of both SAR and numerical wave model information. This is essential not only for practical applications in marine design, but also for an understanding of ocean wave physics, as well as for the assimilation of numerical forecast wave models. The scheme is available for ERS-2 SAR and ENVISAT ASAR WM data and also has potential value for use with data from ESA's future Sentinel-1 mission.

The cross-spectra estimated from SAR complex data are used as input for the PARSA scheme. The basic principles and estimation of SAR cross spectra are introduced in the following section.

3.1 SAR cross spectra

A SAR requires a finite period of time, on the order of 1 s (e.g. for C-band SARs), to collect data forming the synthetic aperture. As such, individual looks can be extracted from the Doppler spectrum during the integration time or aperture synthesizing period. Propagation of ocean waves during the short period can be resolved by taking advantage of the phase information in different looks; for instance, the 180° ambiguity of ocean wave travel direction can be eliminated using the SLCS approach (Engen and Johnsen 1995, Lehner *et al.* 2000).

The SAR cross spectrum $\Phi_{I^1, I^2}^{\Delta t}$ is defined as the Fourier spectrum of the cross covariance function ρ_{I^1, I^2} of two SAR looks with separation time Δt

$$\Phi_{I^1, I^2}^{\Delta t} = F\left(\rho_{I^1, I^2}\right). \quad (1)$$

The cross spectrum is a complex valued function with symmetric real and anti-symmetric imaginary parts. The positive peaks of the imaginary part indicate the propagation direction of the waves.

Two individual looks derived from one ERS-2 SAR WM imagette acquired on 28 November 1998 over a North Pacific storm (Li *et al.* 2008) are shown in figure 2(a) and (b). The real and imaginary parts of the cross spectrum computed from the two looks are presented in (c) and (d), respectively. Negative spectral values in the imaginary part of the cross spectra are marked by blue lines. The black lines for the positive values indicate the direction of propagation of ocean waves. Two wave systems with wavelengths around 300 and 420 m are observed in the cross spectrum, indicating a mixed sea state consisting of fully-developed wind sea and long swell systems.

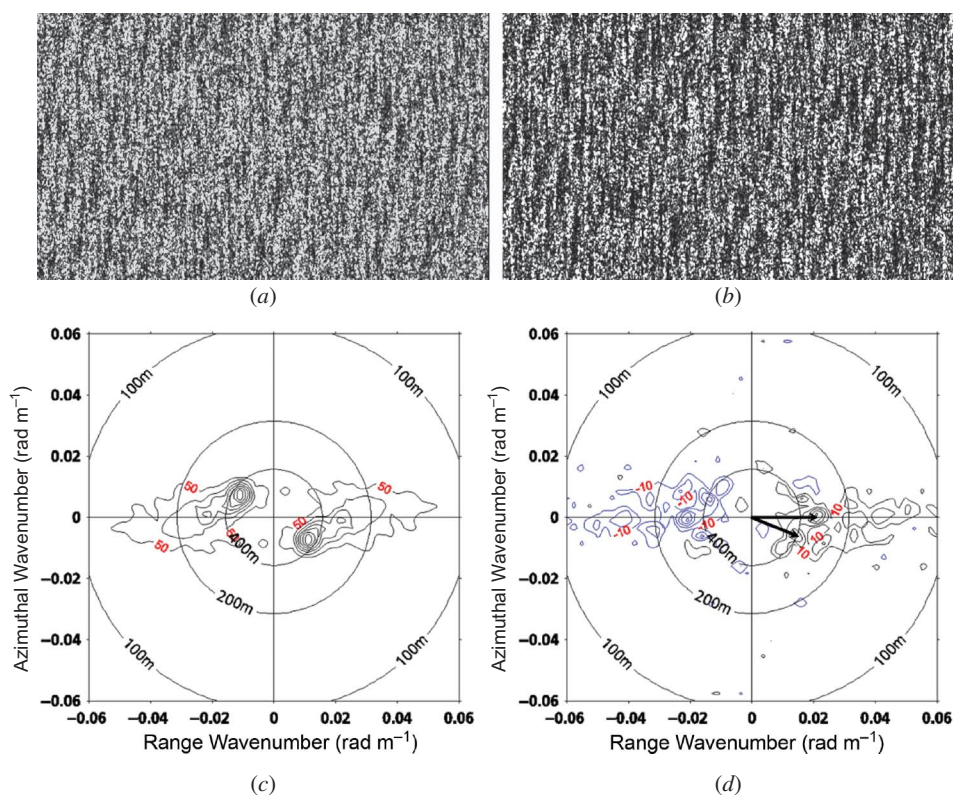


Figure 2. (a) and (b) two individual quicklooks (8 bit grey scale) of one ERS-2 SAR wave mode data acquired on 28 November 1998 over the North Pacific storm. The real (c) and imaginary parts (d) of the cross spectrum are computed from the two looks.

3.2 Non-linear mapping of ocean wave spectra into SAR cross spectra

An integral transform relates the ocean wave spectrum F_k to the SAR cross spectrum of the two looks I^1, I^2 with separating time Δt as defined in Engen and Johnsen (1995):

$$\begin{aligned} \Phi_{I^1, I^2}^{\Delta t}(\mathbf{k}) &= \frac{1}{4\pi^2} \exp(-k_x^2 \beta^2 f^v(0)) \cdot \int_{\mathbf{R}^2} \exp(-i \mathbf{kx}) \exp(k_x^2 \beta^2 f^v(\mathbf{x})) \cdot \\ &\quad \times \{1 + f^R(\mathbf{x}) + ik_x \beta (f^{Rv}(\mathbf{x}) - f^{Rv}(-\mathbf{x})) \\ &\quad + k_x^2 \beta^2 [f^{Rv}(\mathbf{x}) - f^{Rv}(0)] [f^{Rv}(-\mathbf{x}) - f^{Rv}(0)]\} d^2\mathbf{x} \end{aligned}$$

The formula for $\Phi_{I^1, I^2}^{\Delta t}$ was already given in (1). Here, $\beta = R/V$ is the ratio of slant range (R) to platform velocity (V), k_x is the azimuth wave number component and the cross-covariance functions f^v, f^{Rv}, f^R are defined as follows:

$$\begin{aligned} sf^R(\mathbf{x}) &= 0.5 \int_{\mathbf{R}^2} \left(F(\mathbf{k}) \cdot |T_k^R|^2 \exp(i\omega\Delta t) + F(-k) \cdot |T_{-k}^R|^2 \exp(-i\omega\Delta t) \right) \exp(i \mathbf{kx}) d^2\mathbf{k} \\ f^{Rv}(\mathbf{x}) &= 0.5 \int_{\mathbf{R}^2} \left(F(\mathbf{k}) \cdot T_k^R (T_k^v)^* \exp(i\omega\Delta t) + F(-k) \cdot T_{-k}^R (T_{-k}^v)^* \exp(-i\omega\Delta t) \right) \exp(i \mathbf{kx}) d^2\mathbf{k} \\ f^v(\mathbf{x}) &= 0.5 \int_{\mathbf{R}^2} \left(F(\mathbf{k}) \cdot |T_k^v|^2 \exp(i\omega\Delta t) + F(-k) \cdot |T_{-k}^v|^2 \exp(-i\omega\Delta t) \right) \exp(i \mathbf{kx}) d^2\mathbf{k} \end{aligned} \tag{3}$$

When Δt is equal to zero for SAR intensity data, (2) describes the non-linear transformation as introduced in Hasselmann and Hasselmann (1991).

The SAR transfer function T^s is given by:

$$T_k^S = T_k^R + i \frac{R}{V} k_x T_k^u \tag{4}$$

T^R is the RAR modulation function, including tilt modulation, hydrodynamic modulation and range bunching.

If one expands only the integral part in (2) to a linear order, then the remaining leading exponential factor yields the quasi-linear transform as given by:

$$\Phi_{I^1, I^2}^{\Delta t}(\mathbf{k}) \approx 0.5 \exp[-k_x^2 \beta^2 f^v(0)] \left(|T_k^S|^2 \exp(i\omega\Delta t) F_k + |T_{-k}^S|^2 \exp(-i\omega\Delta t) F_{-k} \right). \tag{5}$$

The simulated SAR cross spectrum used in the PARSAs inversion is calculated according to the non-linear transformation given in (2).

3.3 PARSAs retrieval strategy

The PARSAs inversion scheme requires first guess information, e.g. from the numerical wave model WAM, and uses complex information of SAR data to eliminate the ambiguity related to the direction of wave propagation. Details on the structure and numerical procedure of the inversion scheme were outlined in Schulz-Stellenfleth *et al.* (2005). In the present paper, only the main points of the PARSAs scheme are provided as a general overview.

Compared to the non-linear MPI inversion scheme, PARSAs has several additional features.

- In addition to the three parameters used to adjust wavelength (or wave number), wave energy and propagation direction in the different wave systems in the prior spectra, another parameter is used to describe the directional spreading of wave systems.
- The algorithm is based on explicit models for the measurement error, errors in the forward mapping model, and uncertainties in the prior wave spectrum.

The following model is used in the PARSA approach for derivation between the simulated and observed cross spectra due to errors in the SAR imaging model:

$$\Phi_k^{\text{obs}} = \alpha_1 \exp[-k_x^2 \alpha_2] \Phi_k^{\text{sim}} + \varepsilon_k^F. \quad (6)$$

α_1 describes errors in the overall energy level of the spectrum. α_2 describes uncertainties in the SAR ocean wave forward model and ε^F is regarded as the error due to the estimation of the SAR cross spectrum.

3.3.1 Uncertainties in the prior wave spectrum. The approach uses the SAR information to adjust parameters such as wavelength, wave height, propagation direction and directional spreading in the prior spectrum F_k from the numerical wave model, e.g. the WAM model.

Considering that F_k can be split into n_p different sub wave systems S^i using a partitioning scheme, a stochastic model with vector $(X_E^i, X_k^i, X_\Phi^i, X_{\Delta\Phi})$ is used for each sub wave system to quantify the confidence of wave height (energy), wavelength (wave number), propagation direction and directional spreading (the same for all sub-systems). Therefore, a partitioned prior spectrum S^i is given on a polar grid (k, Φ) , and the corresponding processes \tilde{S}^i can be written as

$$\tilde{S}^i(\Phi, k) = X_E^i X_{\Delta\Phi} X_k^i S^i(\Phi_0 + (\Phi - X_\Phi^i - \Phi_0) X_{\Delta\Phi}, X_k^i k) \quad i = 0, \dots, n_p. \quad (7)$$

The algorithm makes use of the phase information contained in the SAR cross spectrum to resolve ambiguities in the direction of wave propagation.

The inversion scheme is capable of blending SAR information (cross spectrum, Φ_k) and the wave model spectrum (F_k) in a consistent way based on a maximum posterior approach which maximizes the conditional probability of the retrieved wave spectrum given the SAR measurement and the prior information. Using Bayes theorem the respective probability density function (*pdf*) can be written as

$$pdf(F_k, \alpha | \Phi_k) = \frac{pdf(\Phi_k | F_k, \alpha) pdf(\alpha) pdf(F_k)}{pdf(\Phi_k)}. \quad (8)$$

The symbol α represents a set of uncertain SAR ocean wave imaging parameters, as introduced in (6). A flowchart for the inversion scheme is given in figure 3.

The first step for the inversion scheme is to decompose the prior wave model spectrum F_k into different wave systems, e.g. windsea and swell, by using the transformation given in (7). The maximum posteriori approach is equivalent to a cost function minimization, which is solved using an iterative approach to estimate an ocean wave spectrum such that the respective simulated cross spectrum as calculated by the fully non-linear forward model best matches the measured cross spectrum.

4. Validation and intercomparison for PARSA scheme results and WWV products

In this section, validation procedures and results for the PARSA scheme are presented. Integral wave parameters derived from inverted two-dimensional wave

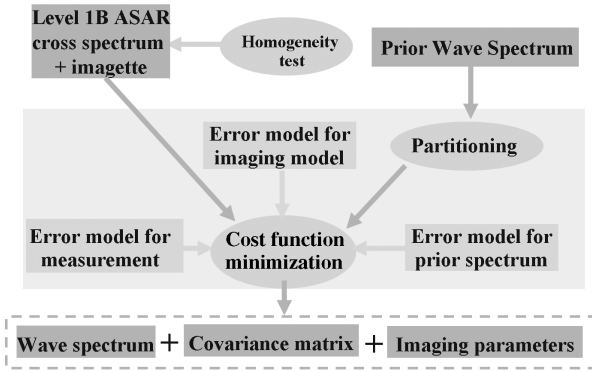


Figure 3. Flowchart of the PARSA algorithm.

spectra by using the PARSA scheme are compared to *in situ* buoy measurements and results from the ECMWF reanalysis wave model and the DWD forecast wave model.

ASAR WM WW products are also validated for comparison in the present study.

Three individual PARSA spectra chosen from different sea states are compared to the WWV wave spectra and the collocated ECMWF wave model spectra to demonstrate the differences of inverted wave spectra from the ASAR WM data by using the two schemes.

4.1 Validation of integral wave parameters retrieved by PARSA and WWV

The integral wave parameters, e.g. SWH, T_{m02} and H_{12} , can be derived from the estimated two-dimensional ocean wave spectra by:

$$SWH = 4 \sqrt{\int E(f, \theta) df d\theta} \tag{9}$$

$$T_{m02} = \sqrt{\int \int E(f, \theta) df d\theta / \int E(f, \theta) f^2 df d\theta} \tag{10}$$

$$H_{12} = 4 \sqrt{\int_{f < 1/12s} E(f) df d\theta} \tag{11}$$

H_{12} , given in (11), is associated with wave components with wavelengths longer than 220 m in deep water. Such waves are easily detectable as patterns on the ASAR images.

To quantify the differences between ASAR measurements Y_i and observations X_i (buoy or numerical model), bias, root-mean-square-error (RMSE) and the scatter index (SI) are used. The bias is removed when determining the SI calculation, as shown in (12):

$$SI = \frac{1}{\bar{X}_i} \sqrt{\frac{1}{n} \sum \left[(Y_i - \bar{Y}_i) - (X_i - \bar{X}_i) \right]^2} \tag{12}$$

4.1.1 Validation of the PARSA scheme. We compare the wave parameters integrated from the PARSA spectra, i.e. SWH, H_{12} , T_{m02} , mean wave frequency and mean wave direction, to numerical wave models, *in situ* buoy and RA measurements.

SWH derived from PARSA spectra in December 2006 and January, February and May 2007 are compared to *in situ* buoy measurements. There are a total of 1247 data pairs collocated. The location of the buoys is given in Appendix 1.

Scatter diagrams in figure 4(a) and (b) show SWH derived from PARSA spectra and the ECMWF reanalysis wave model against buoy measurements, respectively. The colourful squares in the diagrams indicate the data pair density in number within a box of 0.25 m on both axes.

For the model-derived SWH comparison, only cases collocated to PARSA retrievals are considered. Due to the assimilation of ASAR (through MPI scheme) and RA observations, the correlation of the ECMWF model's SWH with buoy measurement is in good agreement, as indicated by the SI of 20%. The PARSA results have a SI of 21% and an RMS error of 0.64 m, slightly higher than the ECMWF reanalysis wave model's comparison of 0.58 m.

With regard to the comparisons to numerical wave models, data pairs collected during December 2006 to February 2007 are used. SWH values retrieved by PARSA are compared to the ECMWF reanalysis wave model and the DWD forecast wave model. The diagrams are presented in figure 5(a) and (b), respectively.

The comparison shows that the PARSA results have better agreement with the ECMWF reanalysis wave model results than with those of the DWD model; the SI is lower than 10% and the RMS error is 0.25 m, which might be because PARSA uses the ECMWF model results as prior information. As the DWD wave model is independent of SAR and RA information, comparison to this model gives an independent assessment for the PARSA inversion scheme.

One interesting point is that the SWH derived from PARSA spectra is substantially higher than values obtained from both wave models in high sea states. Due to the

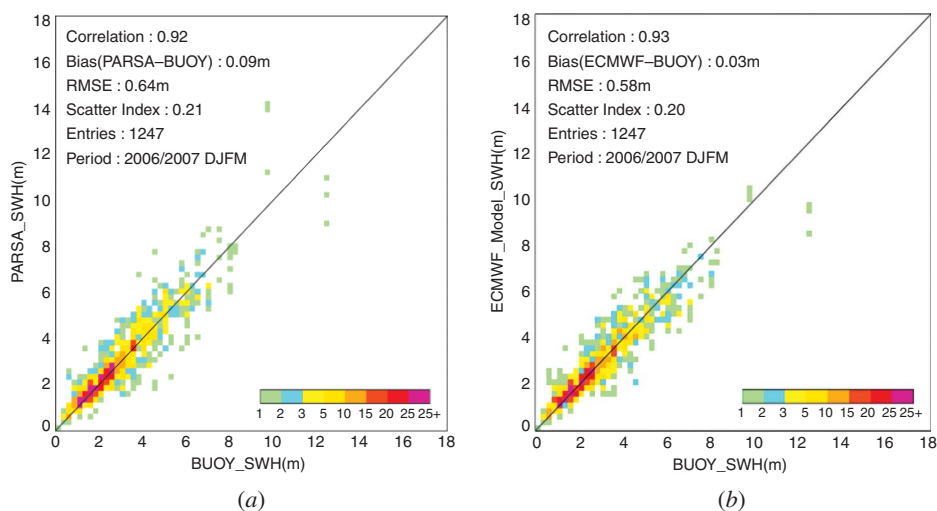


Figure 4. Comparisons of PARSA (a) and collocated ECMWF reanalysis wave model (b) SWH to *in situ* buoy measurements.

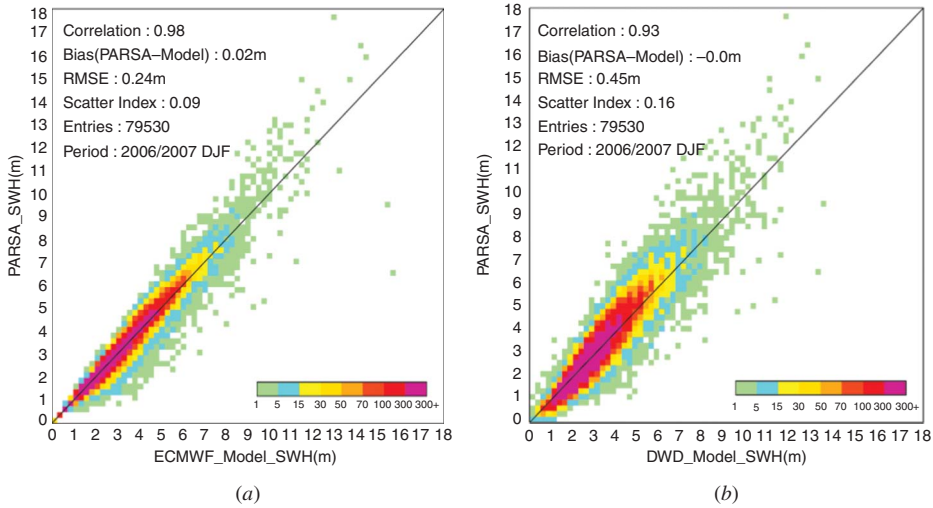


Figure 5. Comparisons of PARSA SWH to results of the ECMWF reanalysis wave model (a) and the DWD forecast wave model (b).

limited buoy comparison in high sea states (as shown in figure 4), it is difficult to judge the quality of PARSA retrieval and the numerical wave model under this situation. Therefore, we use another independent measurement from RA for our comparisons. Figure 6(a) and (b) shows the PARSA SWH compared to the cross-over measurements of GFO and JASON, respectively. The distance between ASAR WM and RA less than 100 km and a collocation time less than 1 h are taken to be as the criteria for collecting cross-over measurements. Both comparisons show that SWH inverted by the PARSA scheme corresponds very well to the RA measurements. The SI is only

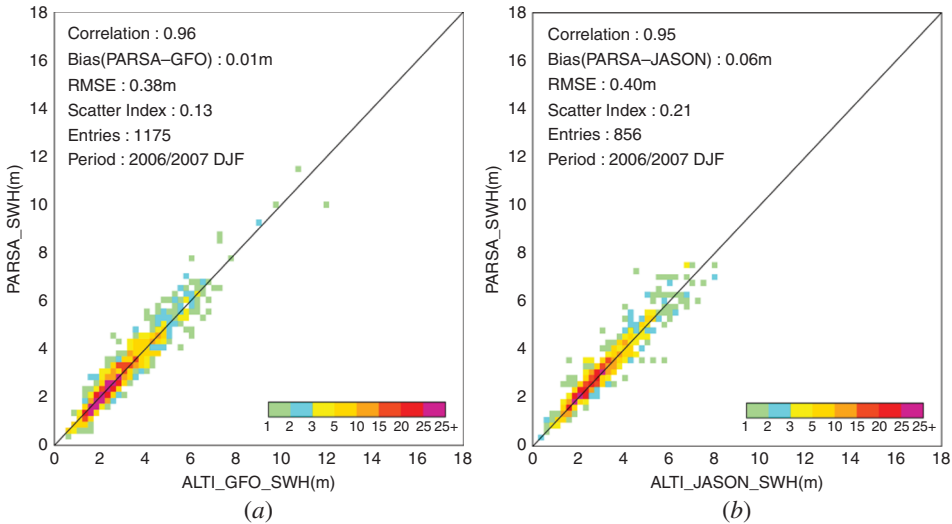


Figure 6. Comparisons of PARSA SWH to cross-over measurements of the radar altimeters GFO (a) and JASON (b).

13% and 12% for comparisons to GFO and JASON, respectively. Although there are few match-up data entries in high sea state, we still find that inverted SWH by using the PARSA scheme yields results very similar to GFO and JASON measurements when SWH is above 8.0 m. An extended dataset is needed for further validation for cases of extreme sea state.

As SAR images particularly long waves, we extract the swell wave height from the inverted PARSA spectra for our tests. Figure 7 shows a comparison of PARSA H_{12} to the results from the ECMWF numerical wave model. The RMSE is 0.26 m and the SI is 24%. When the swell height is greater than 6 m, the inverted H_{12} is generally higher than the hindcast of the ECMWF wave model.

The comparison of PARSA T_{m02} with values from the ECMWF wave model is shown in figure 8. The inverted mean wave period has a reasonably good agreement with the results of the wave model. The bias is 0.08 s and the SI is only 6%. The lowest mean wave period retrieved by PARSA is around 3 s, which corresponds to a wavelength of 15 m in deep water. One can observe many entries showing a higher estimation of mean wave period in PARSA than in the ECMWF wave model results in the range of 5–10 s.

Figure 9(a) and (b) shows the comparison of mean wave frequency and mean wave direction between PARSA spectra and ECMWF wave model spectra. The comparison of mean wave frequency shows reasonably good agreement with a very small bias of -0.001 Hz and an SI of only 6%. The mean wave direction also shows overall agreement with the model results, although there are quite a number of cases with large differences. This might be due to the ‘instantaneous effect’ for sea surface SAR imaging; ASAR acquires one imagette in every 100 km along its orbit during a very

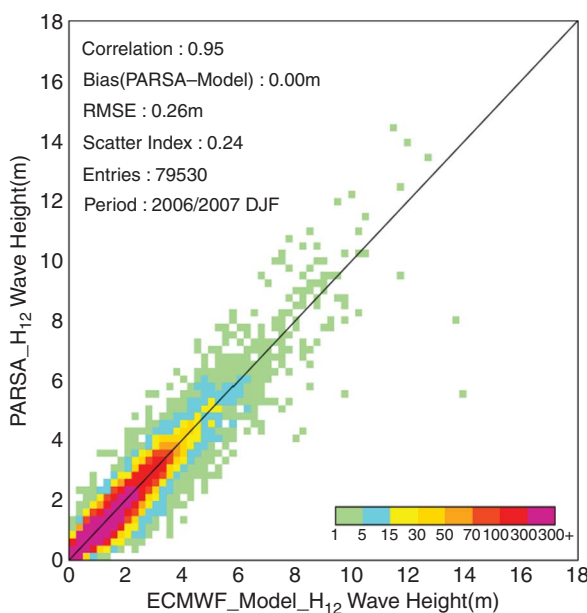


Figure 7. Comparisons of PARSA H_{12} to results from the ECMWF reanalysis wave model.

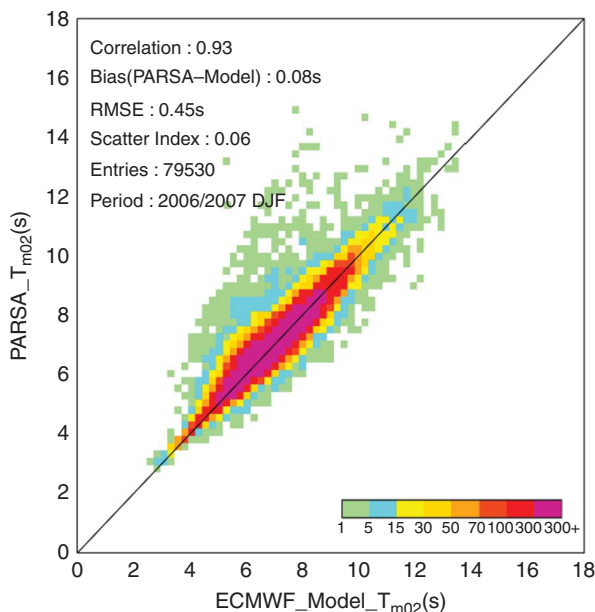


Figure 8. Comparisons of PARSAT_{m02} to results from the ECMWF reanalysis wave model.

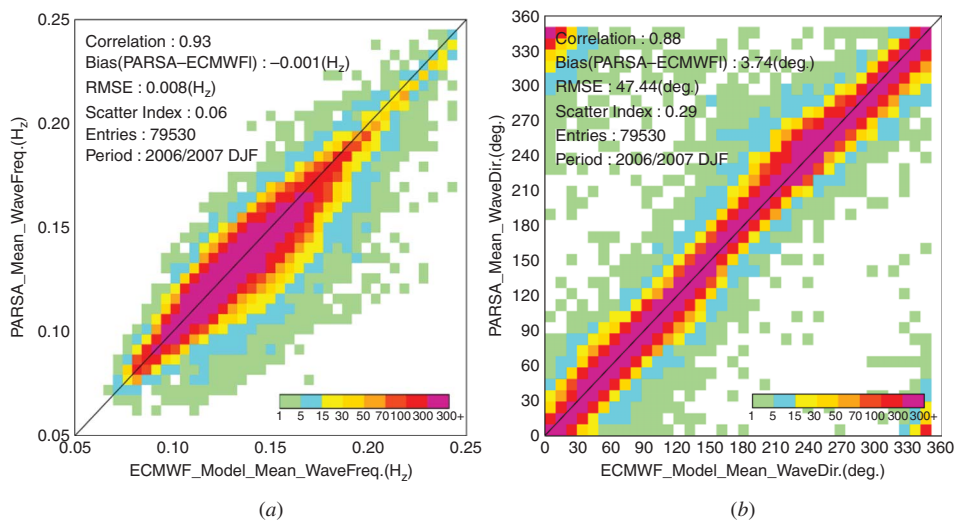


Figure 9. Comparisons of PARSAT mean frequency (a) and mean wave direction (b) to results of the ECMWF reanalysis wave model.

short period of time, which indeed shows the natural variability of surface waves, particularly when it comes to wave direction. In comparison, models provide a smooth forecast or hindcast result over a period of 3 or 6 h.

Integral wave parameters derived from the retrieved two-dimensional ocean wave spectra by the non-linear PARSAT scheme are presented above. We also extract the sea

state parameters from the provided WVV products during the same period (December 2006 to February 2007) to validate the existing scheme in order to derive ocean wave spectra from the ASAR WM data.

4.1.2 Validation of ASAR WM WVV product. In this section, ENVISAT ASAR WVV products are compared to numerical wave models and *in situ* measurements to demonstrate the benefits of PARSA with respect to the currently available operational WVV products. The WVV two-dimensional ocean wave spectra are provided on a log-polar grid with 24 wavelengths and 36 directions. They are intended to deliver particularly precise information for long waves within the cut-off of the spectrum. Thus, the swell wave height H_{12} is also used for assessment here.

A plot of the SWH of WVV products against *in situ* measurements is shown in figure 10. A negative bias of 0.22 m, an RMS error of 0.96 m and a SI of 33% are found in the comparison. When compared to results from the numerical wave models, i.e. the ECMWF and DWD models, the negative bias of around 0.2 m also indicates low estimation of SWH integrated from the WVV wave spectra, as shown in figure 11(a) and (b).

In figure 12, H_{12} values extracted from the WVV product are compared to values from the ECMWF wave model. The SI increased to 43%, whereas the RMSE reduces to 0.48 m and a positive bias of 0.11 m is achieved in the comparison. It could be argued that the WVV results are only useful for the long wave information resolved by the ASAR sensor. Nevertheless, as evident from the H_{12} comparison shown in figure 12, the existing high level WM product (WVV) still cannot provide reliable sea state estimations of swell wave height in many cases, even for waves already longer than 220 m.

The dataset used in the validation of WVV products is the same as the one used to validate the PARSA scheme. However, the data entries in figures 10–12 are fewer than

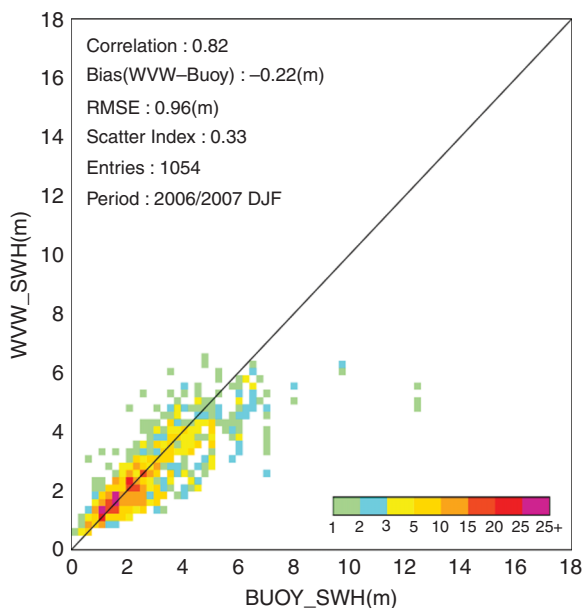


Figure 10. Comparison of WVV SWH to *in situ* buoy measurements.

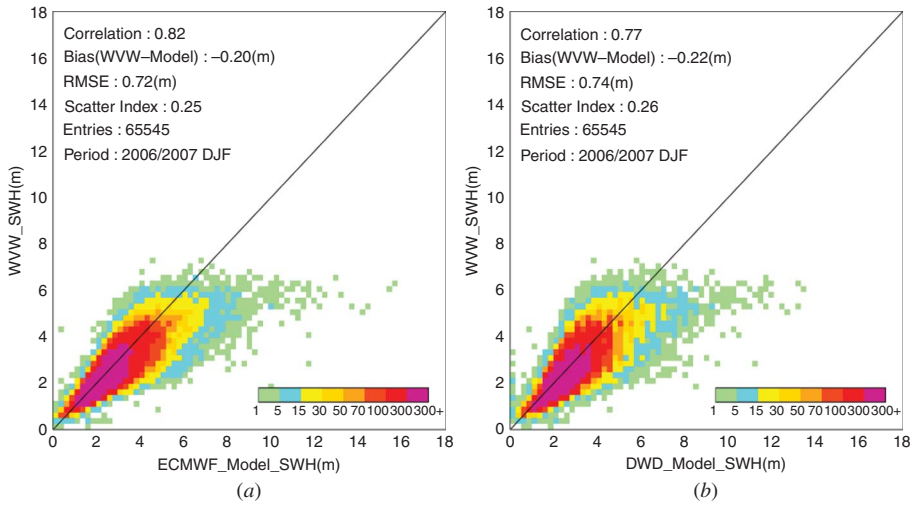


Figure 11. Comparison of WWV SWH to results from the ECMWF reanalysis wave model (a) and the DWD forecast wave model (b).

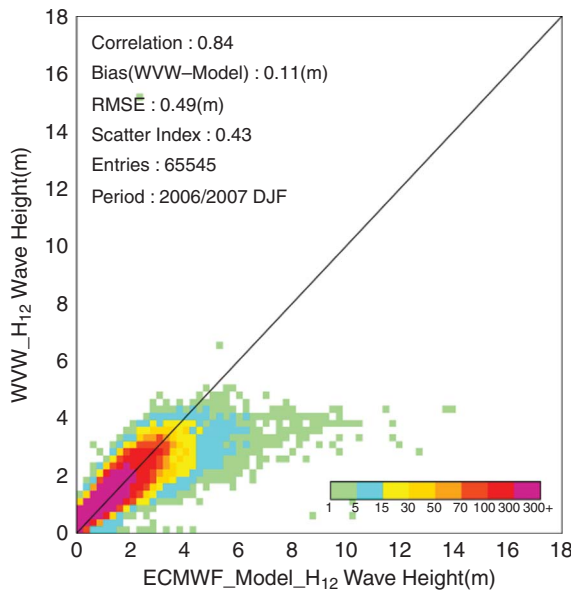


Figure 12. Comparison of WWV H₁₂ to results from the ECMWF reanalysis wave model.

the entries used in figures 4–6. These cases, in which the WWV products are not available (i.e. cannot provide sea state measurements), are excluded from the validations.

Furthermore, considering all the comparisons of wave height (total sea and swell part) derived from the WWV product and PARSA spectra, one can find an obvious underestimation (or saturation) of SWH provided in the WWV product, particularly when SWH is above 5 m.

The validation of integral wave parameters derived from WWV spectra shows that there is a significant limitation for the WWV algorithm. The inverted wave spectra are limited to the SAR cut-off wavenumber domain, not the full two-dimensional ocean wave spectra. Therefore, this results the integrated wave parameters in a significant underestimation, particularly in high sea state, e.g. when SWH is above 5 m or wind speed $> 10 \text{ m s}^{-1}$. This saturation effect is mainly caused by the azimuth cut-off, which is closely related to the local wind speed and wave height.

Using prior information from numerical wave models, the PARSA scheme can yield the full two-dimensional ocean wave spectra and retain the consistency with the results of numerical wave model. On the other hand, the ocean surface wave information contained in SAR blends well into the retrieved spectra.

4.1.3 Comparison to the empirical algorithm CWAVE_ENV. The validation of the non-linear PARSA inversion scheme and the existing ASAR WM WWV product has been demonstrated above. If one is considering the derivation of integral wave parameters directly from ASAR wave mode data without using prior information, the empirical algorithm CWAVE_ENV is suitable (Li, 2010). Validation of the CWAVE_ENV empirical algorithm shows a bias of 0.05 m, RMSE of 0.72 m and SI of 24% when compared to the *in situ* buoy measurements with the same dataset for the PARSA and WWV scheme validation.

In this section, SWH and T_{m02} derived from the PARSA and CWAVE_ENV algorithms are compared. Scatter diagrams in figure 13(a) and (b) present results for the comparisons of SWH and T_{m02} , respectively. One can observe that the empirical algorithm CWAVE_ENV yields a reliable estimation of sea state even without first guess information. SWH derived from the PARSA inversion shows a higher estimation than the results of CWAVE_ENV in extremely high sea states, e.g. SWH higher than 10 m. For extreme sea state, validation of both SAR algorithms is needed as different SAR algorithms and models all behave quite differently. More differences

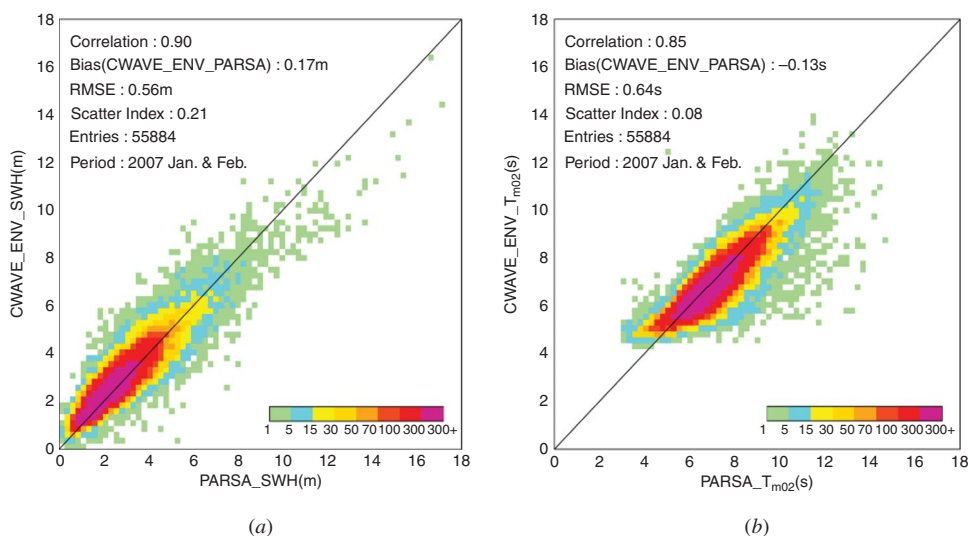


Figure 13. SWH (a) and T_{m02} (b) derived by the PARSA inversion scheme compared with those obtained by using CWAVE_ENV algorithm.

are observed in the comparison of mean wave period derived using both SAR algorithms as shown in figure 13(b). T_{m02} estimated by using the PARSA algorithm is higher than the ones estimated by the CWAVE_ENV algorithm, particular in the period range of 5–10 s. This result is similar to the comparison shown in figure 8, in which the period derived by PARSA is also higher than the model’s results.

4.2 Comparison of individual two-dimensional ocean wave spectra

Both inversion schemes, PARSA and WWV, are used in retrieving two-dimensional ocean wave spectra from SAR WM data. The quality of the inverted two-dimensional wave spectra has been assessed based on the integrated wave parameters.

In this section, a case study is presented with the aim of demonstrating the differences between individual inverted spectra and the collocated wave model spectra.

In figure 14, SWH at 9:00 UTC given by the DWD global forecast wave model on 4 December 2006 is superimposed with one ASAR orbit acquired across the North Pacific between 09:15 UTC and 09:31 UTC. Small squares show the location where ASAR wave mode data are acquired, with colours presenting the SWH retrieved by the PARSA scheme. One can observe that the satellite sub track cuts through a North Pacific storm, yielding a SWH above 10 m. Three ASAR WM imagerettes in this orbit that were located in quite different sea states are used for comparison: A (41° 10' N, 175° 33' W), B (37° 38' N, 174° 36' W) and C (19° 54' N, 170° 22' W), with SWH of 7.6, 5.8 and 2.7 m, respectively, as given by the PARSA inversion.

Respective two-dimensional ocean wave spectra retrieved from the three ASAR imagerettes, as well as the wave spectra derived from the ECMWF reanalysis wave model used as prior information for PARSA scheme, are shown in figure 15(a), (b) and (c), respectively.

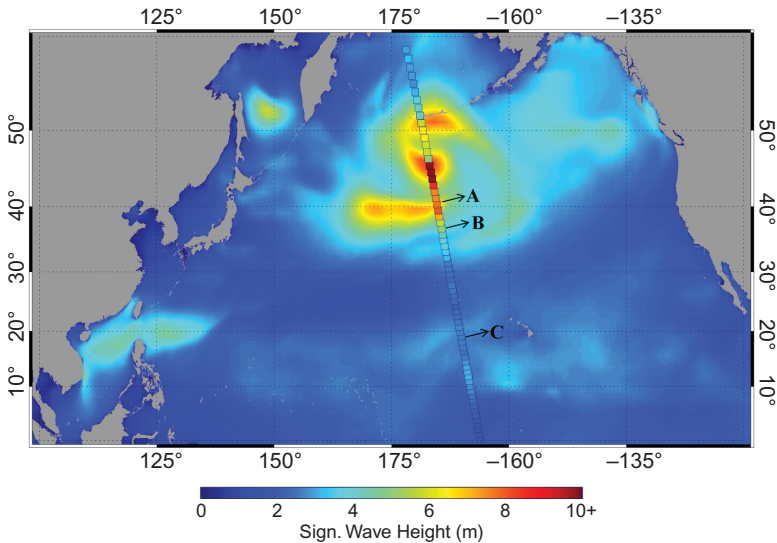


Figure 14. SWH from the DWD forecast wave model on 4 December 2006 at 09:00 UTC superimposed with SWH derived from ASAR WM data by using the PARSA scheme. Locations of three ASAR imagerettes chosen for individual comparison (as shown in figure 15) are labelled.

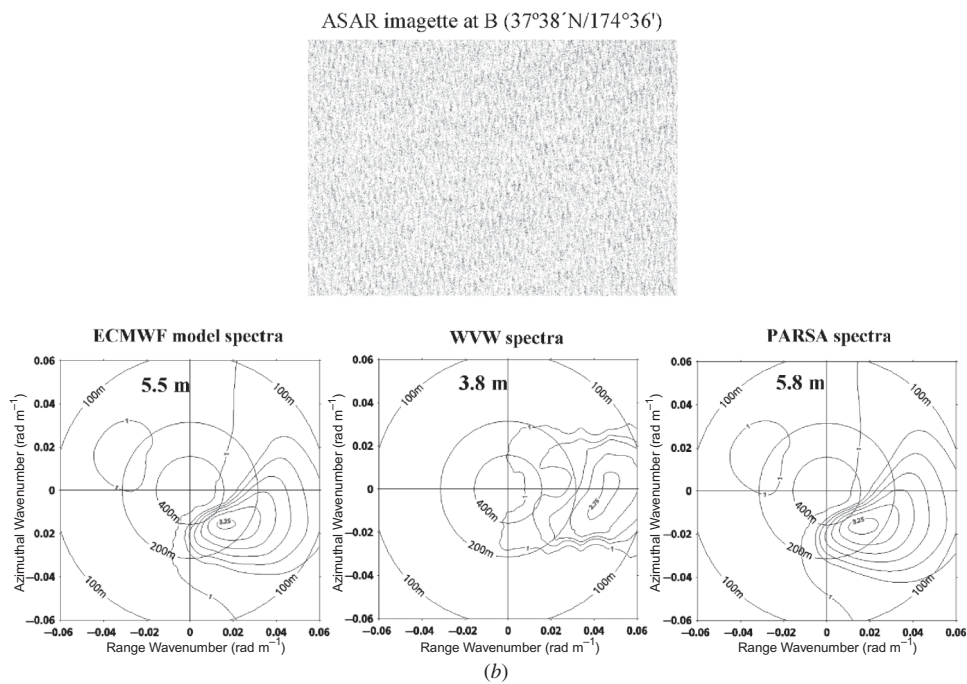
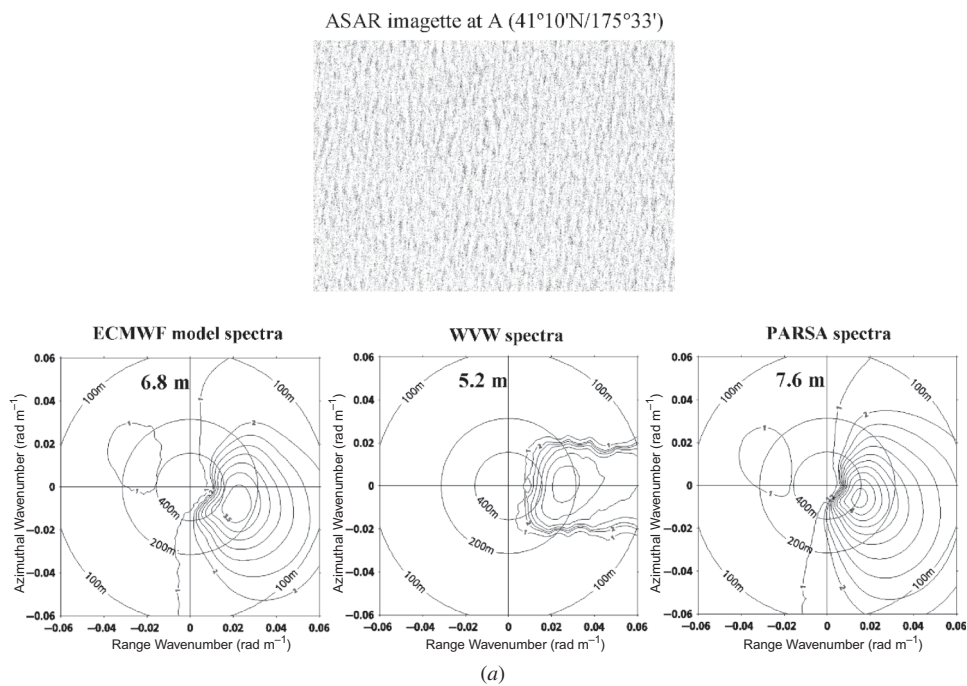


Figure 15. Respective quicklooks (all scaled in 8 bit grey scale) of ASAR imagettes (© ESA), ECMWF wave model spectrum, ESA WVW spectrum and PARSA spectrum for A (a), B (b) and C (c).

ASAR imagette at C (19°54'N/170°22')

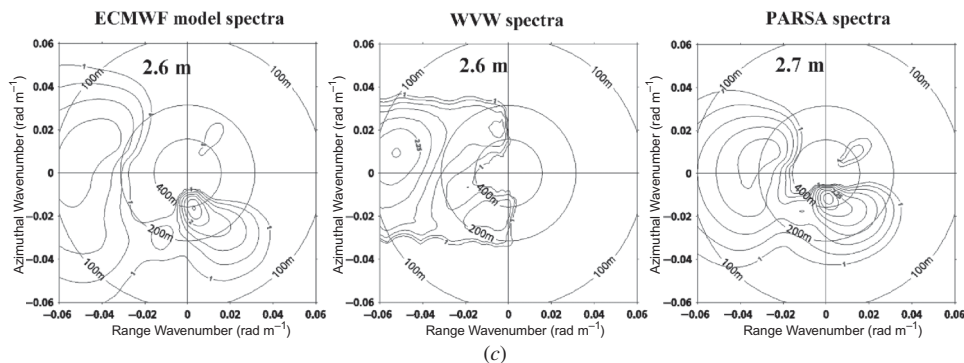
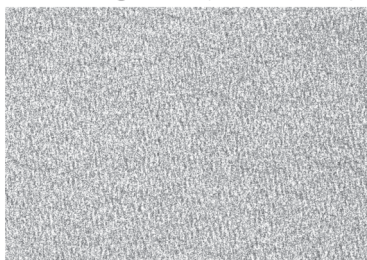


Figure 15. (Continued.)

The retrieved PARSA spectra are consistent with the prior wave model spectra. In the retrieved PARSA spectra, compared to the prior model spectra, the adjusted wave energy, wavelength and propagation direction, as well as the directional spreading can be observed. For ASAR imagette A, two swell systems with peak wavelength of 200 m and 300 m are resolved by the ECMWF reanalysis wave model. The later swell system with higher energy is adjusted by the PARSA inversion scheme to an increased wavelength of around 400 m. The energy adjustment causes the model's SWH of 6.8 m to increase to 7.6 m by the PARSA scheme. With respect to ASAR imagette B, it appears that the SWH increases only slightly from 5.5 m (ECMWF) to 5.8 m, as given by the PARSA result. ASAR imagette C is located in the region with a mixed sea state. Four wave components travelling in different directions are observed in wave spectra. Peak wavelengths for these subsystems are all increased by the PARSA inversion, while the SWH remains consistent for the total sea as compared to the prior information. From a comparison of the three examples, it can be generally concluded that the PARSA scheme blends the ASAR observations into the prior information in a homogeneous way with adjustments for partitioned wave systems. These adjustments increase with the sea state; for example, the adjustment for the energy is especially high in high sea states.

The ocean wave spectra derived from ASAR wave mode WWV products are obviously limited to the ASAR cut-off wavenumber, i.e. short wave information is missed in the azimuth direction. Only the long wave information contained in the ASAR image is retrieved. On the other hand, it can observe that artificial effects of SAR ocean wave imaging are also visible in the cross spectra; these need to be addressed when using the SAR look cross spectra to resolve the direction of wave propagation.

Through the comparison of individual wave spectra, one can generally conclude that the shape of individual spectra differ somewhat between the PARSA spectra and the ECMWF numerical wave model spectra. Differences also arise in peak wavelength and wave direction, as well as in spectral width, although the sea state parameters integrated from these spectra may have good agreement.

5. Summary and conclusions

Two schemes, PARSA and WWV, aiming at the retrieval of two-dimensional wave spectra from ASAR WM data are validated using the data acquired from December 2006 to February 2007 and during one additional month in May 2007. Both schemes use the same inputs, ASAR WM level-1b WVS product (i.e. the SAR cross spectra), for inversions. We compare the integrated wave parameters in terms of SWH (for total sea and swell), T_{m02} , mean wave direction and frequency, to *in situ* measurements, results from the numerical wave models, and measurements of RA. Individual wave spectra acquired in different sea states are also examined to demonstrate differences in the shape of spectra between SAR inverted and hindcast wave model. The following conclusions may be drawn from the validation study:

- (1) The PARSA scheme is proposed for deriving full two-dimensional ocean wave spectra from the SAR WM data. The integrated wave parameters from PARSA spectra, e.g. SWH for total sea, T_{m02} , mean wave direction and mean wave frequency, are used to assess the quality of the inverted spectra.

A summary of the statistical parameters obtained in these comparisons given in table 1 (second row), in terms of SWH. Validation shows that stable SWH are achieved using the PARSA inversion scheme. Comparisons to *in situ* buoy measurements and to results from the DWD forecast wave model allow for independent assessments. Both comparisons show that the bias is negligible, with SI of 21% and 16%, respectively.

The available high level wave product of ASAR WM data, WWV, can only achieve wave measurements resolved within the SAR cut-off. Therefore, the integrated wave height from the WWV product is significantly underestimated and scatter indices are higher than 30%.

For this study, we did not use any restrictions in filtering WWV products from the validation dataset. It must be noted the different filters, e.g. the wave height filter: difference between observed SWH and model SWH less than 5.0 m as used by Li and Holt (2009), the wind speed filter: wind speed less than 8 m s^{-1} in Collard *et al.* (2009), and probably some other filters not mentioned (Johnson *et al.* 2002), have a profound influence on the statistics.

Table 1. Statistical results of different SAR ocean wave algorithms for SWH compared with *in situ* buoy measurements and numerical wave models.

Algorithm	vs buoy			vs ECMWF			vs DWD		
	Bias (m)	RMSE (m)	SI	Bias (m)	RMSE (m)	SI	Bias (m)	RMSE (m)	SI
PARSA	0.09	0.64	0.21	0.01	0.25	0.09	-0.01	0.46	0.16
WWV	-0.19	0.88	0.36	-0.16	0.65	0.30	-0.19	0.67	0.31

In addition to the wave height and wave period, we also compare the mean wave direction extracted from the PARSA spectra to the results of the ECMWF model. Dominant entries show agreement of mean wave direction between the PARSA spectra and the reanalysis of ECMWF wave model, although there are a number of cases presenting differences of more than 90° . The sea surface is recognized mathematically as the sum of individual waves travelling in different directions, which vary constantly. ASAR WM measurements are acquired every 100 km along the orbit, which represent instantaneous sampling over the sea surface, whereas the model provides a homogeneous sea state. This may explain the differences between ASAR observations and models and may also indicate the natural variability of ocean waves.

- (2) We further examine the swell wave height, H_{12} , extracted from the WVV products. However the comparison also reveals a significant underestimation for swell wave height, as shown in figure 10. A similar result is achieved in assessment of long-term quality, as validated in the ECMWF (Abdalla *et al.* 2008).
- (3) Saturation of SWH estimated by the WVV product is most likely caused by the cut-off effect of SAR imaging of ocean waves. This effect limits the inverted WVV spectra to the cut-off; however, this parameter (cut-off wavelength), relates to local wind speed, as well as sea state, which in turn can be used to retrieve wind speed or wind sea information. This is a reasonable explanation as to why the CWAVE_ENV algorithm can yield full sea state measurements even without using prior information, as presented in §4.2.4.
- (4) It should also be noted that currently, the *in situ* dataset does not contain any data from the Southern Hemisphere, where high sea states are observed in large regions throughout the year and where the PARSA scheme can particularly improve knowledge of ocean surface waves. Another issue addressed was the fact that most of the buoys are close to the coast and are therefore not fully representative of the sea state (in particular for storm events) in the open ocean. One strategy presented is the use of matched-up altimeter measurements. We conducted the comparison of the PARSA SWH to the cross-over measurements derived from the JASON and GFO altimeters. The PARSA SWH achieved very good agreement when compared to GFO and JASON, with SI of only 13% and 12%, respectively.
- (5) In addition to the comparisons of SWH, we also conduct comparisons of mean zero upcrossing wave period, mean wave frequency and mean wave direction. Higher estimation is observed in the inverted PARSA T_{m02} when compared results of the ECMWF reanalysis wave model and the CWAVE_ENV algorithm. Further comparisons to *in situ* buoy measurements are needed for validating the SAR algorithms to derive mean wave period.
- (6) Comparison of individual inverted two-dimensional wave spectra by the PARSA inversion to the ECMWF wave model spectra indicates that the inverted PARSA spectra do well at blending the SAR information into the prior wave model results, leading to the adjustment in the wave direction, and wavelength as well as wave energy. This change increases with sea state, which is especially obvious for the wave height.

In the present study, the ECMWF reanalysis wave model assimilated with wave observations is used as the first guess information for the PARSAs inversions. In further work, a forecast wave model without assimilated wave observations (e.g. the DWD forecast wave model), used as the priori will be considered.

Acknowledgements

The ASAR wave mode Level-1b and Level-2 products and collocated *in situ* buoy measurements and ECMWF reanalysis wave model data are collected from Ifremer/CERSAT via Project OSIRIS, funded by ESA. We are grateful to Dr Thomas Bruns for providing the DWD forecast numerical wave model data.

References

- ABDALLA, S., JANSSEN, P.A.E.M. and BIDLOT, J.-R., 2008, Status of global validation of ENVISAT ASAR wave mode products at ECMWF. In *Proceeding of SEASAR Workshop*, ESRIN, Frascati, Italy (Frascati: ESA), ESA-SP656.
- ALPERS, W., ROSS, D.B. and RUFENACH, C.L., 1981, On the detectability of ocean surface waves by real and synthetic aperture radar. *Journal of Geophysical Research*, **86**, pp. 6481–6498.
- BROOKER, G., 1995, UWA processing algorithm specification, version 2.0. Technical Report, European Space Agency, ESTEC/NWP, Noordwijk, The Netherlands.
- CHAPRON, B., JOHNSEN, H. and GARELLO, R., 2001, Wave and wind retrieval from SAR images of the ocean. *Annales des Télécommunications*, **56**, pp. 682–699.
- COLLARD, F., ARDHUIN, F. and CHAPRON, B., 2009, Monitoring and analysis of ocean swell fields from space: new methods for routine observations. *Journal of Geophysical Research*, **114**, C07023, doi: 10.1029/2008JC005215.
- ENGEN, G. and JOHNSEN, H., 1995, SAR-ocean wave inversion using image cross spectra. *IEEE Transactions on Geoscience and Remote Sensing*, **33**, pp. 329–360.
- GOWER, J.F.R., 1983, ‘Layover’ in satellite radar images of ocean waves. *Journal of Geophysical Research*, **88**, 7719–7720.
- GÜNTHER, H., HASSELMANN, S. and JANSSEN, P., 1992, The WAModel cycle 4 (revised version). Technical report 4, Deutsches Klimarechenzentrum (DKRZ), Hamburg, Germany.
- HASSELMANN, K., R.K. RANEY, W.J. PLANT, ALPERS, W., SHUCHMAN, R.A., LYZENGA, D.R., RUFENACH, C.L., and TUCKER, M.J., 1985, Theory of synthetic aperture radar ocean imaging: A MARSEN view. *Journal of Geophysical Research*, **90**, pp. 4659–4686.
- HASSELMANN, K. and HASSELMANN, S., 1991, On the nonlinear mapping of an ocean wave spectrum into a synthetic aperture radar image spectrum and its inversion. *Journal of Geophysical Research*, **96**, pp. 10713–10729.
- HASSELMANN, S., BRÜNING, C., HASSELMANN, K. and HEIMBACH, P., 1996, An improved algorithm for the retrieval of ocean wave spectra from SAR image spectra. *Journal of Geophysical Research*, **101**, pp. 16615–16629.
- HEIMBACH, P., HASSELMANN, S., and HASSELMANN, K., 1998, Statistical analysis and intercomparison with WAM model data of three years of global ERS-1 SAR wave Mode Spectral retrievals. *Journal of Geophysical Research*, **103**, pp. 7931–7977.
- JANSSEN, P.A.E.M., 2008, Progress in ocean wave forecasting. *Journal of Computational Physics*, **227**, pp. 3572–3594.
- JANSSEN, P.A.E.M., ABDALLA, S. and BIDLOT, J.-R., 2007, ENVISAT wind and wave products: monitoring, validation and assimilation. In *Proceeding of ESA-ENVISAT Symposium*, Montreux, Switzerland, ESA-SP636.
- JOHNSEN, H. ENGEN, G., CHAPRON, B., WALKER, N. and CLOSA, J., 2002, Validation of ASAR wave model level 2 product. In *Proceedings of Envisat Validation Workshop*, 9–13 December 2002, Frascati, Italy.

- JOHNSEN, H. and COLLARD, F., 2006, ASAR wave mode – validation of reprocessing upgrade. ESA ESRIN IT Rep. 3/2006 (Frascati: ESA).
- JOHNSEN, H. and COLLARD, F., 2009, Global validation and long-term quality assessment of ASAR wave mode products 2008–2011. ESA/ESRIN IT Rep. 10/2009 (Frascati: ESA).
- KROGSTAD, H.E., 1992, A simple derivation of Hasselmann's nonlinear ocean –synthetic aperture radar transforms. *Journal of Geophysical Research*, **97**, pp. 2421–2425.
- LEHNER, S., SCHULZ-STELLENFLETH, J., SCHÄTTLER, J.B., BREIT, H. and HORSTMANN, J., 2000, Wind and wave measurements using complex ERS-2 wave mode data. *IEEE Transactions Geoscience and Remote Sensing*, **38**, pp. 2246–2257.
- LI, J.-G. and HOLT, M., 2009, Comparison of Envisat ASAR ocean wave spectra with buoy and altimeter data via a wave model. *Journal of Atmospheric and Oceanic Technology*, **26**, pp. 593–614.
- LI, X.-M., LEHNER, S. and HE, M.-X., 2008, Ocean wave measurements based on satellite synthetic aperture radar (SAR) and numerical wave model (WAM) data – extreme sea state and cross sea analysis. *International Journal of Remote Sensing*, **29**, pp. 6403–6416.
- LI, X.-M., 2010, Ocean surface wave measurement using SAR wave mode data. PhD thesis, University of Hamburg, Germany. Available online at: <http://www.sub.uni-hamburg.de/opus/volltexte/2010/4492/>.
- LYZENGA, D.R., SHUCHMAN, R.A. and LYDEN, J.D., 1985, SAR imaging of waves in water and ice: evidence for velocity bunching. Unconstrained inversion of waveheight spectra from SAR images. *Journal of Geophysical Research*, **90**, pp. 1031–1036.
- OUCHI, K., 1988, Synthetic aperture radar imagery of range traveling ocean waves. *IEEE Transactions Geoscience and Remote Sensing*, **26**, pp. 30–37.
- SCHULZ-STELLENFLETH, J. and LEHNER, S., 2004, Measurement of 2-D sea surface elevation fields using complex synthetic aperture radar data. *IEEE Transactions on Geoscience and Remote Sensing*, **42**, pp. 1149–1160.
- SCHULZ-STELLENFLETH, J., LEHNER, S. and HOJA, D., 2005, A parametric scheme for the retrieval of two-dimensional ocean wave spectra from synthetic aperture radar look cross spectra. *Journal of Geophysical Research*, **110**, C05004.1, doi: 10.1029/2004JC002822.
- WAMDI GROUP, 1988, The WAM model a third generation ocean wave prediction model. *Journal of Physical Oceanography*, **18**, pp. 1775–1810.

Appendix 1. List of buoys used for validation

The names, latitudes and longitudes of buoys used for validation are given in table A1. The positions of the buoys are shown in figure A1.

Table A1. Names, latitudes and longitudes of buoys used for validation, corresponding to the red cross marks shown in figure A1.

Station	Latitude	Longitude	Station	Latitude	Longitude
NODC_41 001	34° 44' N	72° 41' W	NODC_51 001	23° 26' N	162° 13' W
NODC_41 002	32° 19' N	75° 22' W	NODC_51 002	17° 11' N	157° 47' W
NODC_41 009	28° 30' N	80° 10' W	NODC_51 003	19° 13' N	160° 49' W
NODC_41 010	28° 57' N	78° 29' W	NODC_51 004	17° 31' N	152° 29' W
NODC_42 001	25° 54' N	89° 40' W	NODC_51 028	0° 01' S	153° 52' W
NODC_42 002	25° 10' N	94° 25' W	NODC_fpsn7	33° 29' N	77° 35' W
NODC_42 003	26° 04' N	85° 56' W	NODC_46 063	34° 16' N	120° 42' W
NODC_42 019	27° 55' N	95° 22' W	NODC_46 066	52° 42' N	154° 59' W
NODC_42 020	26° 56' N	96° 42' W	NODC_46 084	56° 35' N	136° 10' W
NODC_42 035	29° 14' N	94° 25' W	MEDS_C44137	42° 17' N	62° 00' W
NODC_42 036	28° 30' N	84° 31' W	MEDS_C44140	43° 45' N	51° 45' W
NODC_42 039	28° 47' N	86° 01' W	MEDS_C44141	43° 00' N	58° 00' W
NODC_42 040	29° 11' N	88° 13' W	MEDS_C44251	46° 26' N	53° 23' W
NODC_44 004	38° 29' N	70° 26' W	MEDS_C44255	47° 17' N	57° 21' W
NODC_44 008	40° 30' N	69° 26' W	MEDS_C44258	44° 30' N	63° 24' W
NODC_44 011	41° 07' N	66° 35' W	MEDS_C46004	50° 56' N	136° 05' W
NODC_44 014	36° 37' N	74° 50' W	MEDS_C46036	48° 21' N	133° 56' W
NODC_44 025	40° 15' N	73° 10' W	MEDS_C46131	49° 55' N	124° 59' W
NODC_46 002	42° 36' N	130° 16' W	MEDS_C46132	49° 44' N	127° 56' W
NODC_46 005	46° 01' N	130° 58' W	MEDS_C46134	48° 40' N	123° 29' W
NODC_46 011	34° 53' N	120° 52' W	MEDS_C46145	54° 22' N	132° 25' W
NODC_46 012	37° 22' N	122° 53' W	MEDS_C46146	49° 20' N	123° 44' W
NODC_46 013	38° 14' N	123° 19' W	MEDS_C46183	53° 37' N	131° 06' W
NODC_46 014	39° 12' N	123° 58' W	MEDS_C46184	53° 55' N	138° 51' W
NODC_46 015	42° 45' N	124° 51' W	MEDS_C46185	52° 25' N	129° 49' W
NODC_46 022	40° 47' N	124° 32' W	MEDS_C46204	51° 22' N	128° 45' W
NODC_46 023	34° 42' N	120° 58' W	MEDS_C46205	54° 10' N	134° 17' W
NODC_46 025	33° 45' N	119° 05' W	MEDS_C46206	48° 50' N	126° 00' W
NODC_46 027	41° 51' N	124° 23' W	MEDS_C46207	50° 53' N	129° 55' W
NODC_46 028	35° 44' N	121° 53' W	MEDS_C46208	52° 31' N	132° 41' W
NODC_46 029	46° 08' N	124° 31' W	EUROP_41 100	15° 54' N	57° 54' W
NODC_46 035	57° 03' N	177° 35' W	EUROP_41 101	14° 36' N	56° 12' W
NODC_46 042	36° 45' N	122° 25' W	EUROP_62 001	45° 12' N	5° 00' W
NODC_46 047	32° 26' N	119° 32' W	EUROP_62 029	48° 42' N	12° 30' W
NODC_46 050	44° 38' N	124° 30' W	EUROP_62 081	51° 00' N	13° 24' W
NODC_46 053	34° 14' N	119° 52' W	EUROP_62 105	55° 24' N	12° 24' W
NODC_46 059	38° 02' N	130° 00' W	EUROP_62 108	53° 30' N	19° 24' W
NODC_46 061	60° 14' N	146° 50' W	EUROP_62 163	47° 30' N	8° 24' W
			EUROP_64 045	59° 06' N	11° 42' W

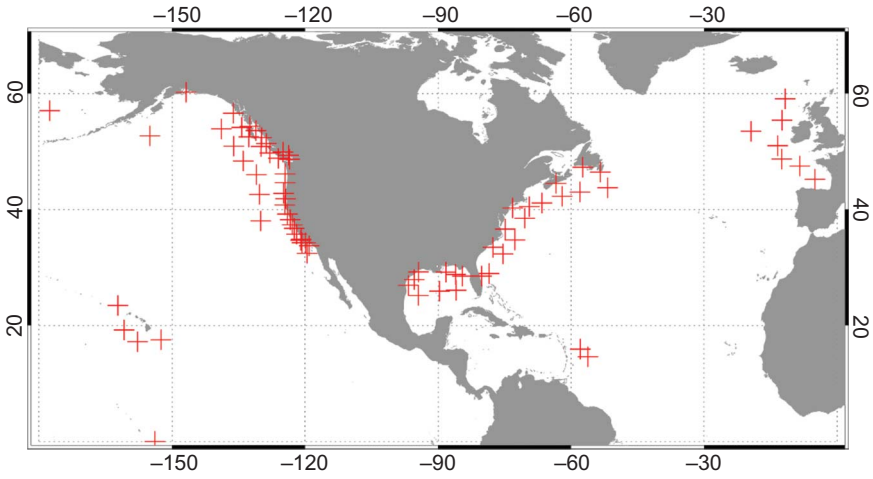


Figure A1. Location of collocated buoys used for CWAVE_ENV model validation.